AGU PUBLICATIONS

JGR

Journal of Geophysical Research: Earth Surface

RESEARCH ARTICLE
10.1002/2014JF003110

Key Points:
- We explored the role of tide and river discharge on 1-D estuarine morphodynamics
- River discharge has impacts by supplying sediment and affecting tidal dynamics
- Stokes drift and river flow enhance ebb residual sediment transport

Correspondence to:
L. Guo,
l.guo@unesco-ihe.org

Citation:
Guo, L., M. van der Wegen, J. A. Roelvink, and Q. He (2014), The role of river flow and tidal asymmetry on 1-D estuarine morphodynamics, *J. Geophys. Res. Earth Surf.*, *119*, 2315–2334, doi:10.1002/2014JF003110.

Received 3 FEB 2014
Accepted 23 SEP 2014
Accepted article online 29 SEP 2014
Published online 4 NOV 2014

The role of river flow and tidal asymmetry on 1-D estuarine morphodynamics

L. Guo[1,2], M. van der Wegen[2,3], J. A. Roelvink[2,3,4], and Q. He[1]

[1]State Key Laboratory of Estuarine and Coastal Research, East China Normal University, Shanghai, China, [2]UNESCO-IHE, Delft, Netherlands, [3]Deltares, Delft, Netherlands, [4]Civil Engineering and Geosciences Faculty, Delft University of Technology, Delft, Netherlands

Abstract Numerous research efforts have been devoted to understanding estuarine morphodynamics under tidal forcing. However, the impact of river discharge on estuarine morphodynamics is insufficiently examined. Inspired by the Yangtze Estuary, this work explores the morphodynamic impact of river discharge in a 560 km long tidal basin based on a 1-D model (Delft3D). The model considers total load sediment transport and employs a morphodynamic updating scheme to achieve long-term morphodynamic evolution. We analyze the role of Stokes drift, tidal asymmetry, and river discharge in generating tidal residual sediment transport. Model results suggest that morphodynamic equilibrium is approached within millennia by vanishing spatial gradients of tidal residual sediment transport. We find that the interaction between ebb-directed Stokes return flow/river flow with tides is an important mechanism that flushes river-supplied sediment seaward. Increasing river discharge does not induce continuously eroded or accreted equilibrium bed profiles because of the balance between riverine sediment supply and sediment flushing to the sea. An intermediate threshold river discharge can be defined which leads to a deepest equilibrium bed profile. As a result, the shape (concavity or convexity) of the equilibrium bed profiles will adapt with the magnitude of river discharge. Overall, this study reveals the significant role of river discharge in controlling estuarine morphodynamics by supplying sediment and reinforcing ebb-directed residual sediment transport.

1. Introduction

1.1. Tidal Hydrodynamics and Sediment Transport

In tide-dominated estuaries, tidal hydrodynamics and associated tidal residual sediment transport determine the morphological changes to a major extent [*Postma*, 1961; *de Swart and Zimmerman*, 2009; *van der Wegen and Roelvink*, 2008, 2012]. Tidal waves propagate into shallow estuaries and are modified by landward width convergence and depth reduction, bottom friction, and river discharge. Depending on the relative importance of the damping and amplifying factors, tidal wave amplitude may increase or decrease or remain constant during the landward wave propagation [*Prandle*, 1985; *Jay*, 1991; *Friedrichs and Aubrey*, 1994; *Lanzoni and Seminara*, 1998; *Savenije*, 2005; *Toffolon and Lanzoni*, 2010]. Depending on the ratio of basin length to tidal wavelength, tidal waves are more progressive in longer basins and have a standing character in shorter basins (i.e., where the basin length is small compared to the tidal wavelength of ~400 km) [*Li and O'Donnell*, 2005]. A basin with physical length of a quarter of the tidal wavelength may even become resonant, leading to extreme landward amplification of tidal waves. Even longer basins (>100 km) allow tidal waves to propagate and eventually damp in the basin [*Gallo and Vinzon*, 2005; *Canestrelli et al*., 2013; *Sassi and Hoitink*, 2013].

Tidal interactions with basin geometry, bathymetry, and river flow lead to asymmetric tides [*LeBlond*, 1991; *Parker*, 1991]. Tidal asymmetry is reflected by imbalanced ebb and flood durations and maximum flow velocities (and associated bed shear stresses) as well as by the generation of an M_4 overtide. Tidal asymmetry is thus measured by an M_4/M_2 amplitude ratio in strength and by a tidal surface phase difference $2M_2$-M_4 in direction. *Friedrichs and Aubrey* [1994] suggested that a $2M_2$-M_4 water surface phase difference between 0 and 180° leads to a flood tidal asymmetry in the sense of higher flood velocities during a shorter flood period and between 180° and 360° to an ebb tidal asymmetry.

Tidal asymmetry can generate significant tidal residual sediment transport [*Dronkers*, 1986; *Parker*, 1991; *van de Kreeke and Robaczewska*, 1993; *Friedrichs and Aubrey*, 1988; *Wang et al*., 1999]. A flood tidal asymmetry causes a landward residual sediment transport (sediment import from the sea), and an ebb tidal asymmetry

leads to a seaward residual sediment transport (sediment export to the sea). A basin is flood dominant in the absence of tidal flats and river discharge because of a relatively shorter rising tide but stronger flood tidal currents [*Speer and Aubrey*, 1985; *Lanzoni and Seminara*, 2002]. A flood tidal asymmetry, however, does not necessarily imply a net landward residual sediment transport [*Brown and Davis*, 2010], because other mechanisms may induce tidal residual sediment transport, such as Stokes drift and river flow [*Dronkers*, 1986; *Lanzoni and Seminara*, 2002; *de Swart and Zimmerman*, 2009]. To avoid confusion, in this work we distinguish flood or ebb tidal asymmetry by tidal wave distortion (i.e., $2\,M_2$-M_4 phase difference) and distinguish flood or ebb transport dominance by net landward or seaward tidal residual sediment transport, respectively.

Stokes drift generates residual currents and transport. Caused by a phase lead or lag between tidal elevation and tidal currents, Stokes drift is present under progressive wave conditions [*Stokes*, 1847; *Dronkers*, 2005; *van Rijn*, 2011]. Stokes drift causes a landward accumulation of water and momentum, resulting in a water level gradient (negative seaward). This water level gradient induces a seaward return flow, termed here Stokes return flow. The Stokes return flow may generate a net seaward sediment transport despite the presence of a flood tidal asymmetry [*van der Wegen and Roelvink*, 2008; *van der Wegen et al*., 2008]. The Stokes drift is typically small in magnitude (~cm/s), and its net effect on residual sediment transport is generally not explored very well.

River discharge has a significant effect on estuarine hydrodynamics and morphology. River discharge damps incoming tidal waves through enhanced tidal friction [*Godin*, 1985; *Savenije*, 2005; *Sassi and Hoitink*, 2013]. River flow constrains landward saltwater intrusion by enlarging ebb currents [*Horrevoets et al*., 2004; *Gallo and Vinzon*, 2005]. River discharge is also one of the dominant mechanisms in exporting river-supplied sediment seaward [*Garel et al*., 2009]. Interactions between river flow and intruding saltwater may lead to significant stratification and density currents, causing a local landward sediment transport [*Dyer*, 1995; *Chant et al*., 2011]. Considering morphology, *Cooper* [1993, 2002] and *Karunarathna* [2010] observed that river discharge and associated river floods are responsible for critical short- to medium-term (i.e., year to decade) estuarine morphological changes. *Nittrouer et al*. [2011] reported contrasting sediment transport and morphodynamic evolution under low and high river flow conditions in the lower Mississippi River. A high river discharge induces seaward increasing sediment transport, whereas a low discharge induces seaward decreasing transport. In the Yangtze Estuary (YE), river discharge supplies a huge amount of sediment to the river mouth where a delta is built up. *Yun* [2004] documented that large river floods may trigger abrupt morphodynamic evolution by initiating channel migration and bifurcations. However, a systematical analysis of the impact of river discharge on estuarine morphodynamics is still lacking.

1.2. Modeling Efforts on Estuarine Morphodynamics

Tidal basin morphodynamics have been widely examined by analytical models (counterpart of numerical models) [*van Dongeren and de Vriend*, 1994; *Schuttelaars and de Swart*, 1996, 2000; *Schramkowski et al*., 2002, 2004]. *Lanzoni and Seminara* [2002] suggested invariant flood tidal asymmetry, landward residual sediment transport, and resultant concave equilibrium bed profile in a tidal estuary with insignificant tidal flat storage and no river discharge. The modeled bed profiles were in good agreement with observations in tidal basins with the same length scale as the western Scheldt estuary and the Venice Lagoon [*Schuttelaars and de Swart*, 2000]. Conversely, convex equilibrium bed profiles were also modeled depending on the nature of tidal asymmetry at the mouth and on the basin geometry [*Schuttelaars and de Swart*, 1996, 2000]. *Schramkowski and de Swart* [2002] studied the impact of external overtides (i.e., M_4) on morphodynamic equilibrium and reported that the equilibrium was sensitive to the phase difference between M_2 and M_4 tides (i.e., $2\,M_2$-M_4). *Todeschini et al*. [2008] reported that a convergent tide-dominated estuary tended to reach an equilibrium length by strong accretion at the landward end. The equilibrium length depends on channel width convergence, tidal amplitude, and bottom friction. In summary, these studies had explored the sensitivities of the initial geometry, overtides, bottom friction, advective and diffusive sediment transport, and sediment availability on estuarine morphodynamics [*de Swart and Zimmerman*, 2009] but not on the sensitivity to river discharge.

Numerical models give similar results to analytical models in terms of longitudinal variations of cross-sectionally averaged depth [*Hibma et al*., 2003a, 2003b, 2004; *van der Wegen et al*., 2008]. And process-based 2-D morphodynamic results compared well with 1-D model results in terms of width-averaged, longitudinal bed profiles [*van der Wegen et al*., 2008; *van der Wegen and Roelvink*, 2008]. Both analytical and numerical modeling studies have focused on tide-dominated environments, whereas the role of river discharge is rarely considered, the

recent work by *Canestrelli et al*. [2013] being an exception. *Canestrelli et al*. [2013] modeled 1-D morphodynamics forced by river discharge and tides in a situation mimicking the Fly River estuary and found that increasing river discharge (and associated higher sediment supply) leads to accretion and vice versa. But the impact of river discharge on long-term estuarine morphodynamics has not yet been systematically explored.

Morphodynamic equilibrium may develop in tide-dominated estuaries only in the long term [*de Swart and Zimmerman*, 2009; *van der Wegen et al*., 2008]. It is reached when maximum flood and ebb velocities are similar and constant along the basin (symmetric tide) so that the tidal residual sediment flux vanishes [*Lanzoni and Seminara*, 2002; *Moore et al*., 2009]. Analytical models have also suggested that multiple morphodynamic equilibria may develop depending on the physical basin length in comparison to tidal wavelength [*Schuttelaars and de Swart*, 2000]. Studies of morphodynamics in long (>100 km) basins are rarely reported, because few real cases are available for reference [*Todeschini et al*., 2008; *Canestrelli et al*., 2013].

The empirical relationship between tidal prism (P, in m^3) and cross-sectional area (A, in m^2) suggests a certain type of morphodynamic equilibrium. This relationship was first derived for tidal inlets [*O'Brien*, 1969; *Jarrett*, 1976] and further extensively examined empirically and theoretically [*van de Kreeke*, 1998; *Townend*, 2005]. *Gao and Collins* [1994], *Friedrichs* [1995], *Lanzoni and Seminara* [2002], and *van der Wegen et al*. [2010] confirmed the validity of a *P-A* relationship not only in tidal inlets but also along a tidal basin. A similar relationship between hydraulic flow parameters (i.e., tidal mean discharge) and cross-sectional area, once established for fluvial regimes [*Leopold et al*., 1964], has also been successfully applied in tidal rivers [*Powell et al*., 2006; *Sassi et al*., 2012]. Application of this hydraulic geometry to modeling results in river-influenced estuaries could help to validate modeling efforts but has not yet been reported.

1.3. Aim and Methodology

The foregoing review indicates that (1) morphodynamics of tide-dominated basins are well studied; (2) morphodynamics of short tidal basins (<100 km) are widely examined, whereas morphodynamics of long tidal basins (longer than tidal wavelength) have been less explored; and (3) river discharge has an important effect on estuarine morphodynamics but the impact has not been studied systematically. Thus, inspired by the long YE where river discharge is significant, this study aims to investigate the role of river discharge on tidal residual sediment transport and associated estuarine morphodynamic behavior in long basins. Use is made of a 1-D morphodynamic model (Delft3D). The sensitivity to external tidal asymmetry and channel width convergence are also considered. We focus on the role of tidal asymmetry, Stokes drift, and river flow (and their interactions), whereas density currents and settling/scour lag effects are left out for future study.

The paper is organized as follows. Section 2 introduces the hydrodynamics and morphology of the YE. Section 3 deals with the model setup and setting of scenarios. Section 4 presents a model validation in the YE and hydrodynamic and morphodynamic results of the schematized model. Section 5 discusses the effect of geometry and the role of river flow in governing residual sediment transport and estuarine morphodynamics. In section 6, we formulate conclusions and suggestions for future studies.

2. The Yangtze Estuary

The Yangtze Estuary, located on the eastern China coast, is the region where the Yangtze River meets the East China Sea. The Yangtze River has an annual mean river discharge of 29,800 m^3/s at Datong which is the tidal wave limit and is 560 km upstream of Changxing (Figures 1 and 2). The multiyear averaged river discharge hydrograph at Datong is characterized by pronounced seasonal variations with a monthly discharge of ~10,000 m^3/s in the dry season between November and April and ~50,000 m^3/s in the wet season between May and October (Figure 2c). Observed extremely low and high daily discharges are 4600 m^3/s and 92,000 m^3/s, indicating large interannual variations [*Zhang et al*., 2010]. The YE is a macrotidal estuary with spring tidal range as large as 4.5 m, and the peak current velocity may be locally as high as 3 m/s [*Chen et al*., 1985]. Despite the large river discharge, the ratio of river discharge to tidal prism at the mouth is approximately 1/10 during moderate fluvial and tidal conditions. The tidal waves propagate landward until Datong, and the tidal flood current limit is located around Jiangyin, 180 km upstream of Changxing under intermediate river flow conditions (Figure 2). Wind waves are of secondary importance in the YE, although monsoon-driven wind and occasional summer typhoons may have a significant effect on estuarine circulation and sedimentation [*Fan et al*., 2006].

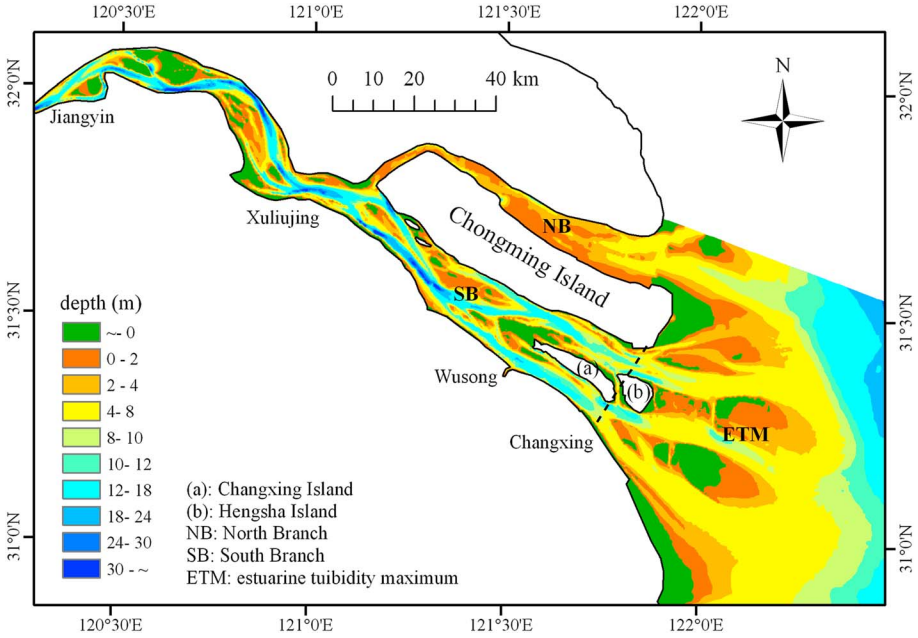

Figure 1. Geometry and bathymetry of the Yangtze Estuary in 1997. Bathymetry (scaled by the color bar) refers to the depth below local datum: lowest normal low water. The dashed line indicates the position of Changxing section.

Tidal waves propagating into the estuary are first amplified in the nearshore area of the YE and decay more landward [*Yun*, 2004]. We analyze tidal water levels by harmonic method in 1 month window during low (dry season) and high (wet season) river discharge periods in 2009. Tidal waves are dominantly damped inside the estuary (upstream of Changxing) despite channel width convergence in the reaches between Jiangyin and Changxing (Figure 3). The landward tidal decay is attributed to combined influences of friction and river discharge. A high river discharge damps tidal waves much more than a low discharge does (Figure 3b). The impact of a high river discharge in causing greater tidal range reduction is consistent with the situation in tidal rivers, in general [*Godin*, 1985; *Gallo and Vinzon*, 2005; *Sassi and Hoitink*, 2013]. Considerable M_4 tide is detected at Changxing (km 560), and its amplitude decreases upstream of Jiangyin (Figure 3a). The surface $2\,M_2$-M_4 phase difference is about 60° at Changxing, suggesting a flood tidal asymmetry with a shorter rising tide.

The YE is complex in both geometry and morphology. Channel bifurcations downstream of Xuliujing lead to four main branches discharging into the sea (Figure 1). Separated from the South Branch near Xuliujing, the

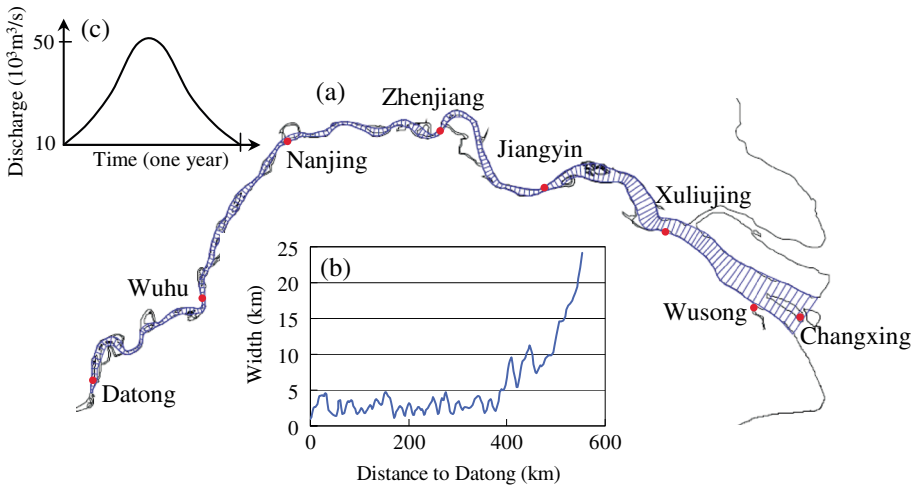

Figure 2. (a) The geometry and (b) width variation of the Yangtze Estuary downstream of Datong, and (c) a sketch of the averaged river discharge hydrograph at Datong.

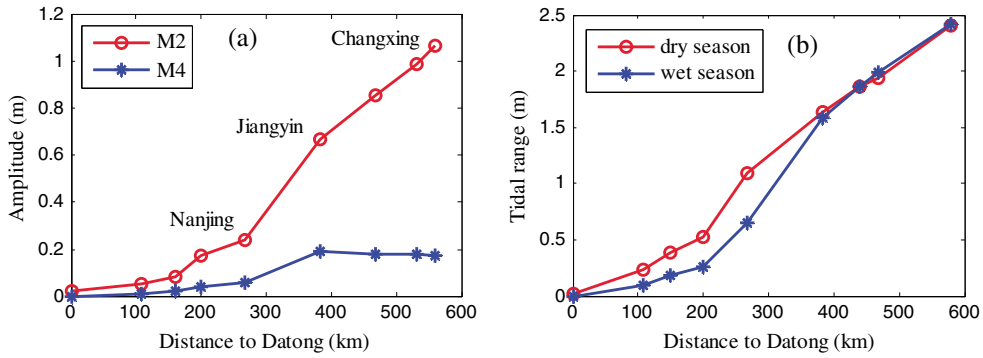

Figure 3. (a) Longitudinal variations of analyzed M_2 and M_4 tidal amplitudes in a wet season and (b) mean tidal range in the dry and wet seasons (data from *Li* [2004]) between Datong and Changxing in the YE.

North Branch nowadays conveys only limited ebb tidal discharge compared to the South Branch. The South Branch is usually a well-mixed (weak stratification) environment and delivers major parts of river flow and sediment to the sea. The bed material upstream of Changxing consists of sand with a median grain size of 150–300 μm [*Liu et al*., 2010]. The estuarine turbidity maximum (ETM) zone seaward of Changxing, dominantly partially mixed, is characterized by three channels and broad tidal flats (Figure 1). Seaward of the ETM, the river flushes into the East China Sea and is subject to alongshore currents induced by shelf circulation [*Liu et al*., 2006]. The formation of the present complex topography in the YE is a result of combined natural processes and human activities. Bank revetments and reclamation of midchannel shoals/sands stabilize the coastlines and channel divisions to a major extent [*Yun*, 2004].

In this study, we focus on the well-mixed reach upstream of Changxing. In the upper 380 km reach, the channel has a relatively uniform width of around 3 km. Downstream of Jiangyin, the channel width expands until the Changxing section where it is 25 km wide (Figure 2). In determining the channel width, the secondary channels formed due to meanders and bifurcations are excluded.

3. Model Setup

This study applies the Delft3D model system in 1-D mode. The model is constructed based on cross-sectionally averaged mass and momentum conservation equations and a long-term morphodynamic updating scheme. *Lesser et al*. [2004] and *Deltares* [2011] provided the details of the hydrodynamics, bed level update schematization, and numerical schemes about the Delft3D model. An important advantage of numerical model is that it takes into account nonlinear processes in the mass and momentum conservation equations (e.g., the friction). Thus, assumptions of linearization are not needed as in many analytical models. This is important for the production of tidal asymmetry which is strongly related to nonlinear processes [*Parker*, 1991; *van Rijn*, 2011]. Another advantage of the numerical model is that the feedback mechanisms between hydrodynamics and morphology are conveniently considered via a robust morphological updating scheme [*Roelvink*, 2006]; hence, longterm (millennia) morphodynamic development is easily achieved.

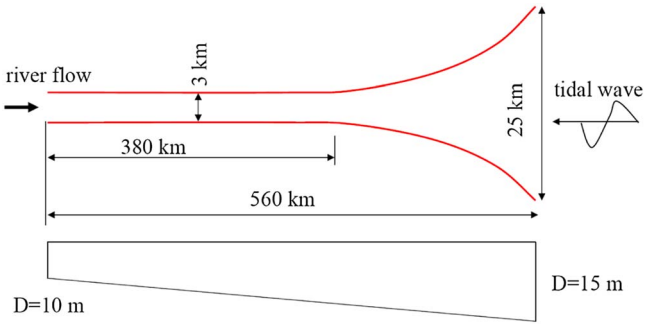

Figure 4. A sketch of the planform and initial bathymetry of the schematized funnel-shaped basin for 1-D model study on a distorted scale.

A 1-D schematized model is constructed by a 560 km long basin with width varying from 3 km (from the landward end to km 380) to 25 km, mimicking the YE outline but excluding meanders and associated channel width variations (Figure 4). This basin is basically longer than tidal wavelength, and the basin width is much larger than the depth; thus, the tidal basin can be considered

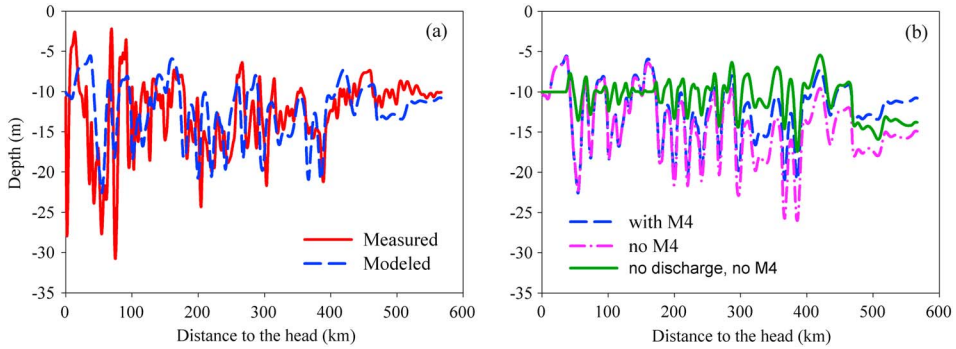

Figure 5. (a) The measured and modeled (after 2000 years) bed profiles in the Yangtze Estuary and (b) the modeled bed profiles after 2000 years in the sensitivity scenarios.

shallow and long [*de Swart and Zimmerman*, 2009]. The length and width of the schematized basin mimic the YE, and the reason for such a long basin is to create continuously landward tidal decay and remove significant tidal wave reflection at the landward end. Regarding initial bathymetry, the modeling study by *Canestrelli et al*. [2013] showed that an initial bathymetry varying in a reasonable range will not induce fundamental differences in the final morphodynamic equilibrium. Therefore, to be consistent with the bathymetry in the YE (see Figure 5a), the initial depth of the schematized model is prescribed by a linearly sloped bed from 10 m at the head to 15 m at the mouth (a slope of 1.12×10^{-5}). Preliminary model runs suggest that these schematizations produce similar tidal damping characteristics as the YE and also lead to stable long-term morphodynamic development.

To focus on the effect of river discharge and tides, the model is primarily forced by river discharge at the landward boundary and tides at the seaward boundary. Only the major tidal component M_2 and its first overtide M_4 are prescribed as representative tides [*Roelvink and Reniers*, 2011]. Estuarine circulation and stratification dynamics are excluded in this 1-D model study, because the river upstream of Changxing in the YE is overall well mixed [*Yun*, 2004] and the region with strong stratification is confined to the utmost downstream part of the estuary [*Xue et al*., 2009]. The channel length featured by stratification (~60 km in the YE) is much shorter than the total estuary length (~600 km in the YE), thus likely not affecting the morphodynamic equilibrium of the whole system [*Canestrelli et al*., 2013].

In line with *van der Wegen and Roelvink* [2008], we define a single sand fraction with the total load transport formula by *Engelund and Hansen* [1967]:

$$S = S_s + S_b = \frac{0.05U^5}{\sqrt{g}C^3\Delta^2 D_{50}} \tag{1}$$

where S_s and S_b are the suspended and bed load transport rates ($m^3/m/s$), U is the current velocity (m/s), C is the Chézy friction parameter ($60\ m^{1/2}/s$), Δ is the relative density defined by $(\rho_s - \rho_w)/\rho_w$, and D_{50} is the median diameter of the bottom material (200 μm). By equation (1), the threshold for initial sediment motion is set to zero implicitly.

Sediment transport boundary conditions are set by an equilibrium sediment flux, which means that riverine sediment supply is unlimited and the sediment load entering or exiting through the boundaries is nearly perfectly adapted to the evolving local flow conditions [*Deltares*, 2011]. By imposing this, the bed level at the landward (inflow) boundary exhibits limited accretion or erosion.

Following *Roelvink* [2006], the model updates bathymetry every hydrodynamic time step. Enhanced morphodynamic updating is achieved by a morphological factor (MF) approach. The MF approach multiplies computed erosion and deposition fluxes along the water-bed interface by a user-defined factor (the MF), thus achieving accelerated bed level changes [*Lesser et al*., 2004; *Roelvink*, 2006]. An important assumption of the MF approach is that bed level changes during one tidal cycle remain limited so that the morphodynamic evolution amplified by an MF will not induce irreversible changes [*Roelvink*, 2006]. This assumption is generally valid other than under extreme conditions (e.g., energetic storm or river floods). The MF approach has been successfully applied in medium- and long-term morphodynamic simulations in various environments [*van der Wegen and Roelvink*, 2008, 2012; *Canestrelli et al*., 2013]. Preliminary simulations

Table 1. Sensitivity Scenarios Defined by Varying River and Tidal Boundary Conditions

			M_4	
Group	Discharge (m^3/s)	M_2 Amplitude (m)	Amplitude (m)	Phase (deg)
1	0–35,000	1.2	0.2	300
2	0–35,000	1.2	0	0
3	0–35,000	1.2	0.2	60
4	0–35,000	0.2	0	0

suggest that an MF up to 400 still gave reliable, numerically robust long-term morphodynamic results with our current 1-D model setup [*van der Wegen et al*., 2008]. Therefore, a 10 year hydrodynamic calculation represents 4000 year morphodynamic evolution which is long enough for the basin to reach a close to equilibrium state.

We design model scenarios by systematically varying the boundary conditions. Following the YE data, the reference case describes an M_2 tide of 1.2 m (phase zero) and an M_4 tide of 0.2 m (phase 300°) at the seaward boundary and a constant river discharge of 30,000 m^3/s at the landward boundary. Sensitivity analyses are conducted by the following: excluding the M_4 tide at the seaward boundary, prescribing a 60° phase for the external M_4 tide at the seaward boundary (reflecting external ebb tidal asymmetry), reducing the M_2 tide to 0.2 m in amplitude to reflect weak tide circumstances, and varying river discharge from 0 to 35,000 m^3/s in increments of 5000 m^3/s.

Simulations are classified into four groups based on varying boundary conditions (Table 1). Group 1, in which the standard case is included, represents the situation with an external M_4 tide implying prescribed flood tidal asymmetry. Group 2 excludes the external M_4 tidal constituent. Group 3 prescribes an external ebb tidal asymmetry. Group 4 has weak tidal forcing thus representing river-dominated circumstance.

We also conduct runs in a 6 km wide rectangular basin with the same length to link with previous similar studies and to test the sensitivity to channel width convergence. All the sensitivity scenarios are run on both convergent and rectangular basins.

We also set up a 1-D model based on a more realistic geometry similar to that between Datong and Changxing in the YE (Figure 2b). The midchannel islands and the North Branch are excluded from the cross-section definition. This realistic model is forced by a river discharge hydrograph characterizing by seasonal discharge variations between 10,000 m^3/s and 50,000 m^3/s (see Figure 2c) and M_2 and M_4 tides ($2M_2$-M_4 is 60°), also mimicking the real situation in the YE. The other model settings, such as sediment transport boundary conditions and initial bed profile, are the same as the schematized model. Morphodynamic sensitivities to river discharge and external tidal asymmetry are examined by running the model excluding a river discharge and an external M_4 tide. Simulation results of the YE model are discussed in section 4.1.

4. Model Results

4.1. YE Morphodynamic Validation

Figure 5 shows the bed profile between Datong and Changxing in the YE in 1997, reflecting cross-sectionally averaged depth. Overall, the bed profile is characterized by slightly larger depth in the middle part. The highly variable depth is caused by channel meanders and width restrictions (e.g., rocky outcrops and bank protection works). The morphodynamic simulation starting from a sloped initial bed shows rapid bed level changes at the beginning. Bed level changes slow down considerably at the end of a 2000 year run, indicating a development toward equilibrium. Eventually, the model produces a bed profile agreeing well with the measured profile after 2000 years (Figure 5a). It demonstrates the ability of a simplified morphodynamic model to produce long-term estuarine bed profiles. The regional discrepancy is attributed to the complexity in the realistic geometry which is not well represented in the schematized 1-D model.

We set up one extra scenario excluding river discharge to test morphodynamic sensitivity to river discharge and one extra scenario excluding the external M_4 tide to test the sensitivity to external tidal asymmetry. Model results indicate that the downstream bed is eroded deeper if no external M_4 tide is prescribed (Figure 5b). This suggests the effect of tide-induced flood transport in counterbalancing river-induced ebb

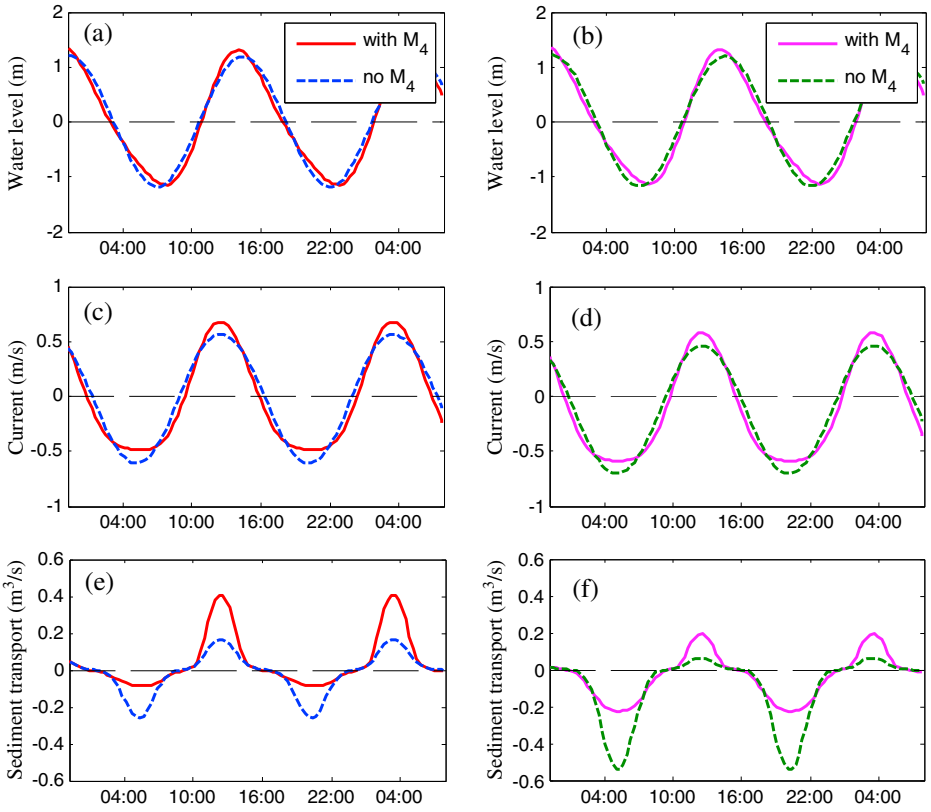

Figure 6. Time series water level, tidal currents, and cross-section integrated sediment transport rate at the mouth section of the convergent estuary for the cases without and with external tide (2 M_2-M_4 is 60°): (a, c, and e) with no river discharge; (b, d, and f) with a discharge of 30,000 m^3/s. Positive is in the flood direction.

transport. Morphodynamic development is much slower and the estuary is less deepened in the middle part in the scenario driven by M_2 tide only (no river discharge and no external M_4 tide) (Figure 5b). That is because residual sediment transport induced by internal tidal asymmetry is relatively small. These sensitivity analyses imply that river discharge and external overtide play a significant role in controlling morphodynamic development in a river- and tide-influenced estuary such as the YE.

4.2. Hydrodynamics of the Schematized Model

We first run four hydrodynamic simulations (no bed level updating) in the schematized convergent estuary in order to develop better insight into the role of the river discharge and tidal asymmetry. Four cases are defined as follows: no river discharge, no M_4 tide (H1); no river discharge, with M_4 tide (2 M_2-M_4 is 60°) (H2); discharge 30,000 m^3/s, no M_4 tide (H3); and discharge 30,000 m^3/s, with M_4 tide (2 M_2-M_4 is 60°, reference case) (H4).

Figure 6 presents the modeled time series of tidal water levels, tidal currents, and cross-section integrated sediment transport at the mouth section. Defining landward (flood direction) transport as positive (throughout this work), the tidal residual sediment transport through the mouth section is estimated by −19 m^3/s (H1), 49 m^3/s (H2), −109 m^3/s (H3), and −39 m^3/s (H4), respectively. The case forced by M_2 tide only (H1) is characterized by a flood tidal asymmetry (shorter rising tide, Figure 6c) but weakly ebb-dominant residual sediment transport (Figure 6e). A prescribed external M_4 tide (H2) further shortens the rising tide period and enlarges the peak flood tidal currents, thus enhancing tidal wave distortion and flood tidal asymmetry and leading to net flood transport dominance. A river discharge as large as 30,000 m^3/s enhances the ebb residual sediment transport (H3 compared to H1), even changes its direction from flood (H2) to ebb (H4). As a whole, comparison of these four preliminary hydrodynamic simulations provides evident differences in tidal residual sediment transport caused by both tidal asymmetry and river discharge.

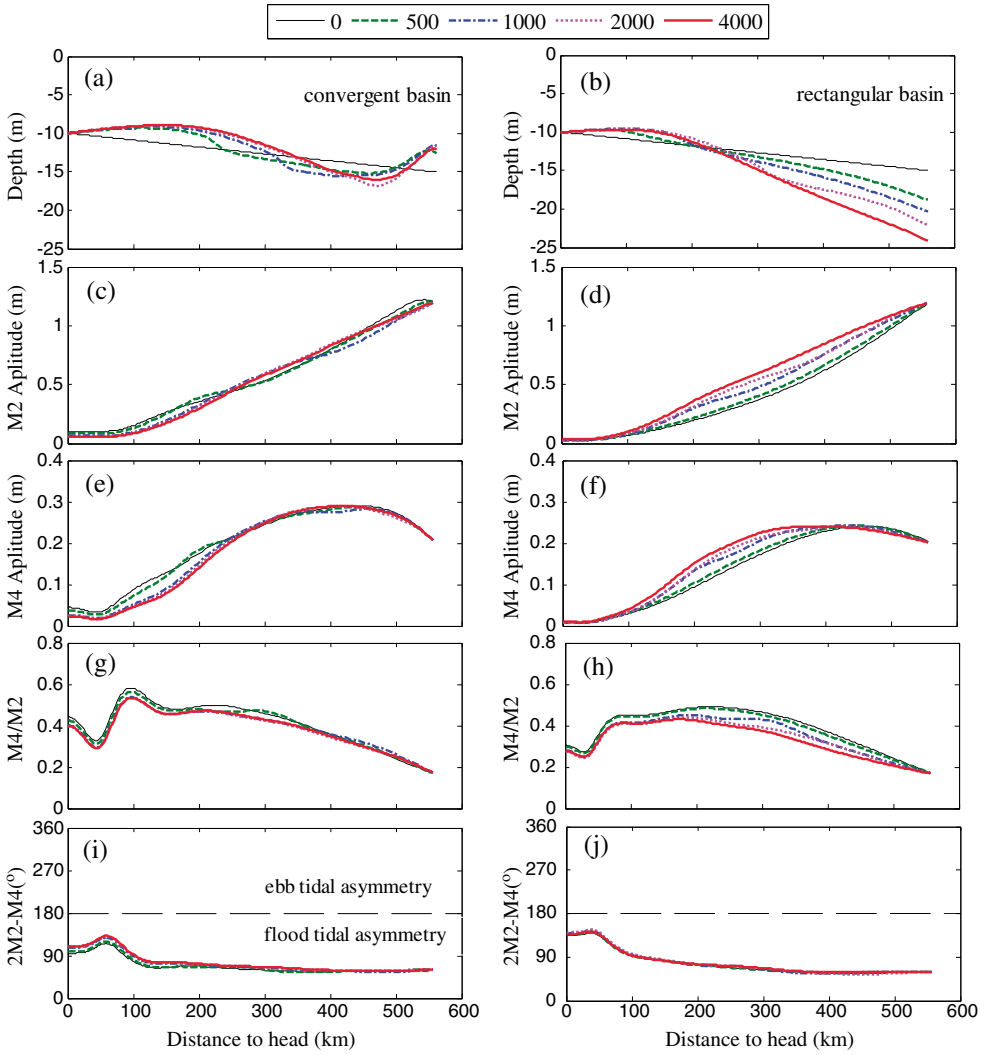

Figure 7. Hydrodynamics and morphodynamic evolution over time (from 0 to 4000 years) of the reference case (i.e., river discharge 30,000 m^3/s and M_4 tide are prescribed) in the convergent and rectangular basins: (a, b) the bed profiles; (c, d) M_2 tidal amplitude; (e, f) M_4 tidal amplitude; (g, h) surface M_4/M_2 amplitude ratio; and (i, j) surface 2 M_2-M_4 phase difference. The thin dashed lines in Figure 7i and 7j differentiate the regions between ebb tidal asymmetry and flood tidal asymmetry.

4.3. Morphodynamics of the Schematized Model

The tidal residual sediment transport discussed in the previous section leads to morphodynamic development once bathymetric updating is allowed. Here we first present the hydrodynamic and morphodynamic results of the reference case (H4) and then of other sensitivity scenarios.

The M_2 tide is damped landward both in the convergent basin and in the rectangular basin (Figures 7c and 7d). The M_4 tide is slightly amplified landward but damps more landward (Figures 7e, and 7f). As a result, the strength of tidal asymmetry (reflected by M_4/M_2 amplitude ratio, Figures 7g and 7h) increases landward to the region about 100 km downstream of the head where fluctuations occur, probably as a result of tidal wave reflection against the landward boundary. The nature of the tidal asymmetry does not change over morphodynamic evolution (Figurea 7i and 7j).

Regarding morphodynamics, the channel bed accretes in the upstream part of the estuary because of excessively supplied sediment by a high river discharge (Figures 7a,and 7b). The convergent basin shows accretion at the mouth due to its widening. Significant channel deepening occurs in the downstream part of the rectangular basin. As a result of the deepened rectangular basin, the M_2 and M_4 tides intrude farther landward over time (Figures 7d and 7f). The M_4 and M_2 tidal amplitudes decrease in the upstream part of the convergent basin because of bed accretion (decreased water depth) (Figures 7c and 7e).

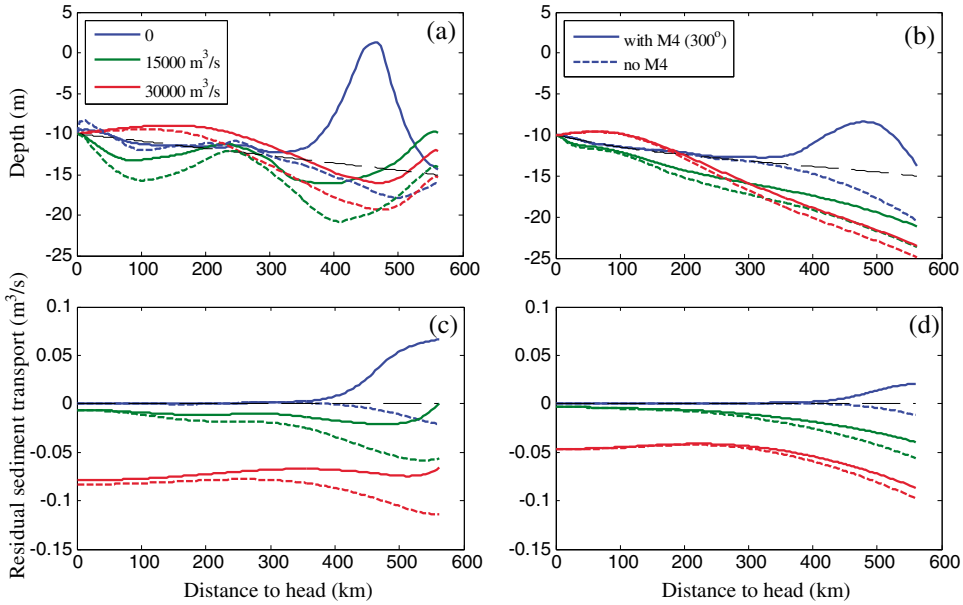

Figure 8. (a, b) Bed profiles after 4000 morphodynamic years and (c, d) tidal residual sediment transport over 4000 years in the convergent basin as shown in Figures 8a and 8c and in the rectangular basin as shown in Figures 8b and 8d. The black dashed lines indicate the initial bed profiles in Figures 8a and 8b and indicate the zero level in Figures 8c and 8d.

Morphodynamic results of other sensitivity scenarios suggest that the variability of the final bed profiles is quite large over a wide range of river discharge and tidal forcing (Figures 8a and 8b). In the absence of a river discharge, the downstream part of the estuary gets deepened in the scenarios without an external M_4 tide and conversely undergoes accretion with an external M_4 tide favoring flood tidal asymmetry. Continued accretion is prone to eventually block the estuary near 450 km in the convergent basin (Figure 8a). A river discharge of 15,000 m^3/s leads to more deepened bed profiles if no external M_4 tide is imposed. A river discharge as large as 30,000 m^3/s causes deepening of the bed profiles in the downstream part of the estuary due to enhanced ebb transport and accretion in the upstream part of the estuary due to excessive riverine sediment input. Furthermore, larger river discharge causes considerable channel accretion and basin infilling because river-supplied sediment is not flushed seaward efficiently (not showed). In comparison to the scenarios without an external M_4 tide, the equilibrium bed profiles in the scenarios considering an external M_4 tide favoring flood tidal asymmetry are overall subject to less deepening. In all, these sensitivity scenarios indicate again that river discharge and tidal asymmetry have a profound effect on long-term estuarine morphodynamics.

4.4. Tidal Residual Sediment Transport

Figures 8c and 8d show tidal residual sediment transport patterns over the entire 4000 morphodynamic years. The tide-dominated scenarios (no river discharge) are characterized by ebb transport dominance in the absence of external M_4 tide. The ebb transport dominance is shifted to flood transport dominance when an external M_4 tide favoring flood tidal asymmetry is prescribed. In correspondence, residual sediment transport is seaward at the mouth section in the former cases, suggesting sediment export to the sea, whereas it is landward in the latter cases, suggesting sediment import from the sea (Figures 8c and 8d). This result is in line with the bed profile development: sediment import leads to accretion in the downstream part of the estuary and conversely sediment export leads to erosion.

Introduction of a river discharge enhances the ebb transport dominance when no external M_4 is imposed. A river discharge also shifts flood transport dominance to ebb transport dominance even when an external M_4 is imposed (Figures 8c and 8d). It means the reinforced ebb transport by a river discharge dominates over the flood-directed transport induced by tidal asymmetry even when an external M_4 tide is prescribed. Note that the residual sediment transport varies greatly along the channel. A seaward positive spatial gradient (seaward decreasing) in the residual sediment transport leads to bed accretion (Figure 8). Conversely, the

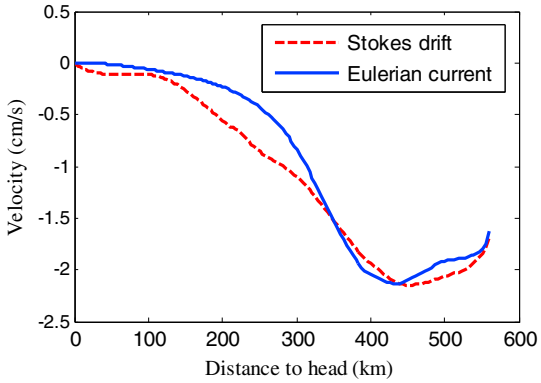

Figure 9. Magnitude of Stokes drift and Eulerian residual currents in the convergent basin driven by only M_2 tide (i.e., no river discharge and no external M_4 tide). Stokes drift is landward (flood direction), and the Eulerian residual currents are seaward (ebb direction).

negative gradient (seaward increasing) in the more seaward channel segment explains the deepening of the estuary.

4.5. Mechanism Analysis

The mechanisms causing tidal residual sediment transport include Stokes drift, tidal asymmetry, and river discharge in this 1-D model study. To explore their contributions to the total residual sediment transport, we decompose the total current into a residual current and periodic M_2 and M_4 tidal currents by

$$U = u_o(x) + u_2(x)\cos(\omega t - kx) + u_4(x)\cos(2\omega t - 2kx + \phi) \quad (2)$$

in which U is the total current, u_o is the residual current, u_2 and u_4 are the amplitudes of the M_2 and M_4 currents, ω and k are the M_2 tidal frequency and wave number, respectively, and ϕ is the velocity $2\,M_2$-M_4 phase difference. Another internally generated overtide, M_6, is smaller in amplitude compared to M_4 thus is excluded in this analysis.

The residual current can be induced by Stokes drift and/or river discharge (if it is present). *Van Rijn* [2011] gives an approximation for the Stokes drift as

$$u_{stokes} = Q/h_o = \left(\int_0^T UH\mathrm{d}t\right)/h_o/T = \left(\int_0^T u\cos\left(\omega t + \phi\right)\left(h_o + \eta\cos\left(\omega t\right)\right)\mathrm{d}t\right)/h_o/T = \frac{1}{2}u\eta\cos\left(\phi\right)/h_o \quad (3)$$

where u_{stokes} is Stokes drift, Q is tidally averaged unit discharge per width, h_o is the mean water depth and T is the tidal period (here 12 h), U is current velocity, H is water depth, $\eta\cos(\omega t)$ is the tide wave and $u\cos(\omega t + \phi)$ is the tidal current with ϕ the phase difference between the vertical and horizontal tides. The presence of Stokes drift and its strength depends on the phase difference ϕ which is 90° for a standing wave and 0° for a progressive wave. Generally the Stokes drift is in the landward direction.

By integrating tidal currents over a tidal period T, we derive tidal residual currents (Eulerian residual current) at each section. In the tide-dominated scenarios, the Eulerian residual currents are seaward (in the ebb flow direction). Its magnitude is nearly the same as the Stokes drift calculated by equation (3) (Figure 9) but in the opposite direction, indicating that the Stokes drift is responsible for the generation of the Eulerian residual current. The tiny discrepancy in Figure 9 may be attributed to ignoring the residual current (u_o) and the M_4 tidal current (u_4) in equation (3). Note that the Stokes drift is overall small in magnitude (order of a few cm/s); it is easily overcome by river discharge-induced seaward residual current.

Regarding residual sediment transport, we propose that the total load transport is proportional to the current velocity by a power of 5 and a zero threshold velocity for initial sediment motion (in line with the *Engelund and Hansen* [1967] formula); thus, the tide-averaged integration is followed as [*Dronkers*, 2005; *van de Kreeke and Robaczewska*, 1993]

$$\begin{aligned}\int_0^T U^5\mathrm{d}t/T &= \int_0^T [u_o(x) + u_2(x)\cos(wt - kx) + u_4(x)\cos(2wt - 2kx + \phi)]^5\mathrm{d}t/T \\ &= \underbrace{u_o^5(x)}_{\mathrm{ENT}} + \underbrace{5u_o^3(x)\left[u_2^2(x) + u_4^2(x)\right] + \frac{15}{8}u_o(x)\ \left[u_2^4(x) + u_4^4(x)\right]}_{\mathrm{EIA}} + \underbrace{\frac{5}{4}u_2^4(x)u_4(x)\cos(\phi)}_{\mathrm{TIA}}\end{aligned} \quad (4)$$

There are three major contributors to the residual sediment transport. The first term in equation (4) is the net transport effect of the Eulerian residual current, termed Eulerian net transport (ENT) here. The second and third terms represent the interactions between the Eulerian residual currents and tidal currents, which have the same direction as the Eulerian residual currents, termed Euler-induced asymmetry (EIA) here. The fourth term is induced by the interaction between M_2 and M_4 tides, reflecting a tide-induced asymmetry (TIA). Its direction is determined by the relative phase difference between the horizontal M_2 and M_4 tides.

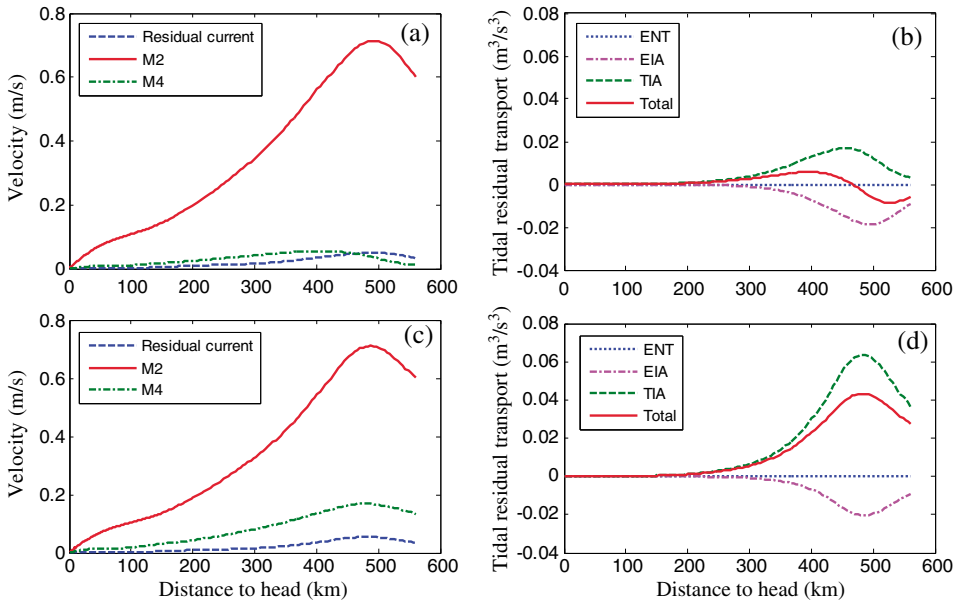

Figure 10. (a, c) Magnitude of M_2 and M_4 tidal currents and residual currents and (b, d) tidal residual sediment transport by ENT, EIA, and TIA, on the initial bathymetry in the tidal scenarios without (Figures 10a and 10b) and with (Figures 10c and 10d) an external M_4 tide favoring a flood tidal asymmetry in the convergent basin.

We estimate the residual sediment transport components by equation (4) based on modeled residual currents and M_2 and M_4 current amplitudes. The Eulerian residual currents and M_4 current are relatively small in the scenarios forced by M_2 tide only (Figure 10a). As a result, ENT is negligible. Residual sediment transport induced by EIA, however, is considerable and is even larger than that by TIA in the utmost mouth section (Figure 10b). It suggests that though the Eulerian residual currents (only Stokes return flow in this case) are small in itself, its interaction with M_2 current is able to generate considerable residual sediment transport. This explains why the internally generated tidal asymmetry is flood directed (flood tidal asymmetry) but the net residual sediment transport is ebb directed (ebb transport dominance) in this circumstance.

Introduction of an external M_4 tide reinforces the M_4 current, making it exceeding the residual currents in magnitude (Figure 10c). As a result, TIA-induced residual sediment transport dominates over the contribution by EIA (Figure 10d), indicating the significance of external overtide. Note that the direction of TIA depends on the external tidal phase relationship $2M_2$-M_4.

Introduction of a river discharge enlarges the Eulerian residual currents significantly, and the Stokes drift becomes relatively minor and can be ignored (Figure 11a). Increasing river discharge enhances both ENT and EIA (termed river-induced asymmetry in this case). A large river discharge may even reverse the net residual sediment transport from flood dominance (due to TIA) to ebb dominance (due to ENT and EIA) (Figure 11b). The ENT is larger in the upstream part of the estuary but EIA and TIA are larger in the downstream. At the mouth, EIA is larger in magnitude than TIA (Figure 11b). In all, the estuary is ebb transport dominant due to the presence of a significant river discharge though tide-induced asymmetry is flood directed.

The EIA generated residual sediment transport depends on the strength of both the Eulerian mean current and the tidal currents. In an estuary driven by a large river discharge but microtidal forcing, small tidal currents will lead to negligible EIA and TIA though the river discharge is large (Figures 11c and 11d). In that case, only the ENT dominates. This reflects the circumstance of a river-dominated estuary in which the seaward residual sediment transport in the downstream part of the estuary (Figure 11d) is much smaller than that in an estuary with both significant river and tidal forcing (Figure 11b).

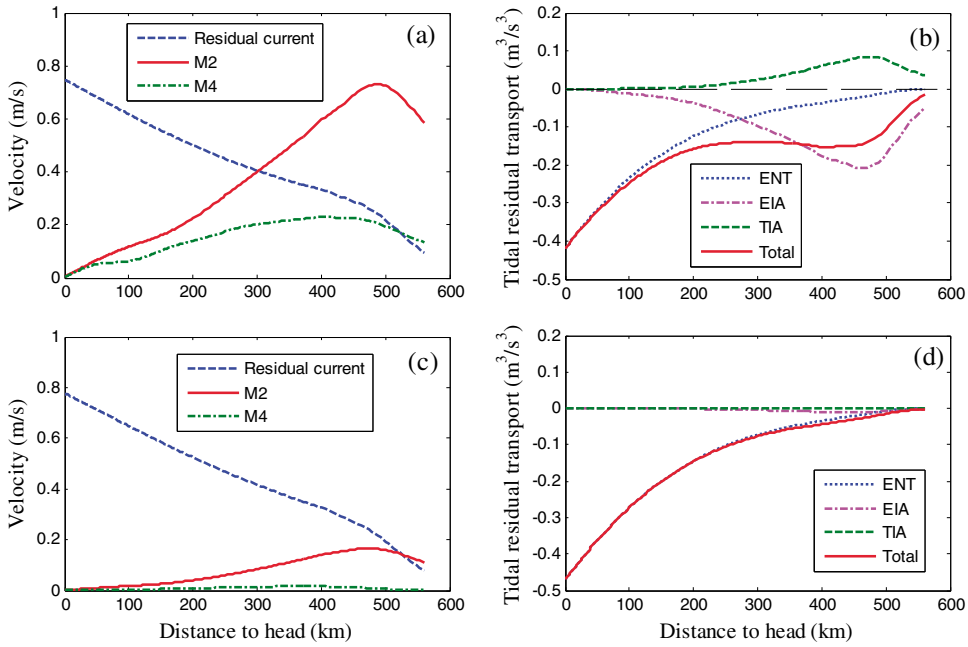

Figure 11. (a, c) Magnitude of M_2 and M_4 tidal currents and residual currents and (b, d) tide residual sediment transport by ENT, EIA, and TIA, on the initial bathymetry in the scenarios (Figures 11a and 11b) with discharge 30,000 m^3/s, normal M_2 and external M_4, and (Figures 11c and 11d) with discharge 30,000 m^3/s but microtidal strength (amplitude of M_2 is 0.2 m) in the convergent basin.

5. Discussion

5.1. Impact of Basin Geometry

Studies of the morphodynamic behavior in relatively short (<100 km) tide-dominated basins are characterized by overall concave profiles due to residual sediment transport divergence (outward transport vectors) [*Friedrichs and Aubrey*, 1994; *Lanzoni and Seminara*, 2002; *Hibma et al*., 2003b; *Schuttelaars and de Swart*, 1996, 2000; *Schramkowski et al*., 2002; *van der Wegen and Roelvink*, 2008]. In this study we derive overall weakly convex profiles in a 560 km long tide-dominated basin because of pronounced ebb transport dominance induced by the interaction between Stokes return flow and tidal currents (see Figure 8b). However, the 100 km long utmost downstream part of the convergent basin is featured by a concave-shaped equilibrium profile. That is because an external M_4 tide favoring flood tidal asymmetry induces persistently landward residual sediment transport (Figure 8a). This result is in line with the findings by *Schramkowski and de Swart* [2002] and *Todeschini et al*. [2008].

Channel width convergence induces regional concavity in the downstream part of the estuary though convexity still dominates in the upstream part of the estuary (uniform width) (see Figure 8a). The regional concavity in the lower stream is similar to that modeled in shorter convergent basins [*Lanzoni and Seminara*, 2002; *Schuttelaars and de Swart*, 2000] and also to the bed profile of the western Scheldt estuary [*Schuttelaars and de Swart*, 2000]. This indicates the effect of channel width convergence in reducing residual sediment transport in the width increased direction. Overall, we find that the channel width convergence only changes the spatial gradients of the tidal residual sediment transport and consequent concavity or convexity in the equilibrium profiles, whereas the direction of the residual sediment transport does not change (see Figure 7).

In tide-dominated circumstances a stronger convergent basin will have a shorter equilibrium basin length and corresponding equilibrium bed profile [*Todeschini et al*., 2008]. The abrupt width expansion in the model of *Canestrelli et al*. [2013] caused strong deposition in the convergent channel. However, it is worthwhile to note that channel convergence in natural settings is shaped by a complex interplay between tidal forcing and bank stability instead of being predefined (nonerodible bank) as in this and previous studies. Further systematic study to explore the interplay between tidal forcing and channel geometry is needed.

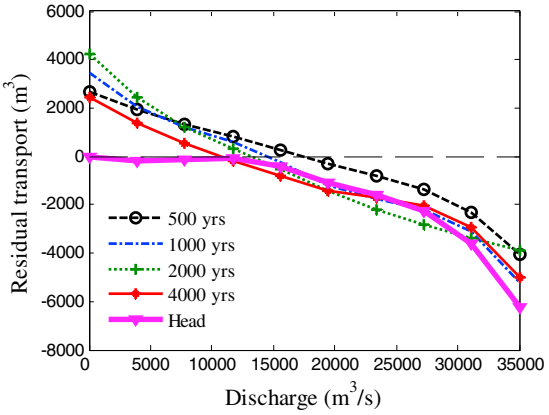

Figure 12. Cross-sectionally integrated residual sediment transport at the mouth section over morphodynamic evolution (in years) and at river head in variation with discharges in the scenarios considering an external M_4 tide favoring flood tidal asymmetry in the convergent basin.

5.2. Role of River Discharge

River discharge supplies sediment, enhances ebb residual flow, alters the tidal hydrodynamics, and interacts with the tidal currents to generate a river-induced asymmetry. Generally, the fluvial effect can be neglected when the river discharge is much smaller than the mean tidal discharge, for instance, when a tidal mean discharge to river discharge ratio is larger than approximately 20 [*Powell et al.*, 2006]. This threshold value may differ per estuary [*Sassi et al.*, 2012], but the concept of a critical river discharge above which the influence of river discharge on the estuarine hydrodynamics and morphodynamics cannot be neglected is valuable.

River discharge significantly enlarges ebb-directed residual current. The river-reinforced residual currents interact with tidal currents, generating significant tidal residual sediment transport in the seaward direction. The river-tide interaction enhances seaward flushing of river-supplied sediment. It can be a dominant mechanism when the residual currents are smaller than the tidal currents.

There is a critical river discharge at which the seaward residual sediment transport (by ENT and EIA) is balanced by landward residual sediment transport (by TIA, given a flood tidal asymmetry) at the mouth section. Figure 12 shows variations of the net residual sediment transport at the head and at the mouth (over time) as a function of river discharge. The residual sediment transport at the mouth is close to zero when river discharge is in the range between 10,000 and 20,000 m^3/s, reflecting a balance between seaward and landward residual sediment transport. A river discharge smaller than this threshold leads to net landward sediment transport (sediment import) and associated channel deposition, whereas a river discharge larger than this threshold causes net seaward transport (sediment export) and associated channel erosion. Note that this threshold discharge increases with increasing tidal asymmetry strength and that no threshold discharge is present if the tide-induced asymmetry is ebb directed.

Continuously increased river discharge does not lead to continuously deepening equilibrium bed profiles. Our morphodynamic model results suggest that when river discharge increases, the equilibrium bed profiles initially become deeper but that further discharge increase (and sediment supply) leads to accreted bed profiles (see Figure 8). Thus, an intermediate river discharge condition can be defined that leads to a deepest equilibrium bed profile. This intermediate condition is characterized by the largest longitudinal residual sediment transport gradient (see Figure 8). A river discharge below this threshold discharge reinforces seaward sediment transport more than the sediment it supplies; thus, the basin becomes deepened. A river discharge above this threshold supplies excessive sediment, and the sediment is not flushed to the sea efficiently; thus, the basin becomes accreted. Depending on basin geometry, tidal asymmetry, and sediment availability, the threshold discharge is also site specific. The nonlinear morphodynamic behavior in response to increasing river discharge suggests that the finding in *Canestrelli et al.* [2013] (i.e., increasing sediment discharge lead to accretion and vice versa) is valid only when river discharge is above the intermediate threshold discharge.

The interaction and strength balance between river and tides governs the state of estuarine morphodynamics in long term if we assume that other factors, e.g., sea level rise and land subsidence, are limited. The concept of strength balance between fluvial and marine forcing is also discussed by *Dalrymple et al.* [1992]. The tidal strength (reflected by tidal amplitude) plays a significant role in this process, because the river-tide interaction depends on the strength of both river discharge and tidal currents. A stronger M_2 tide not only leads to a stronger tide-induced asymmetry but also enhances the river-induced asymmetry (see Figures 11c and 11d). This may explain why the strong tides help to flush river-borne sediment to the sea faster than the sediment is flushed in a purely river-dominated estuary.

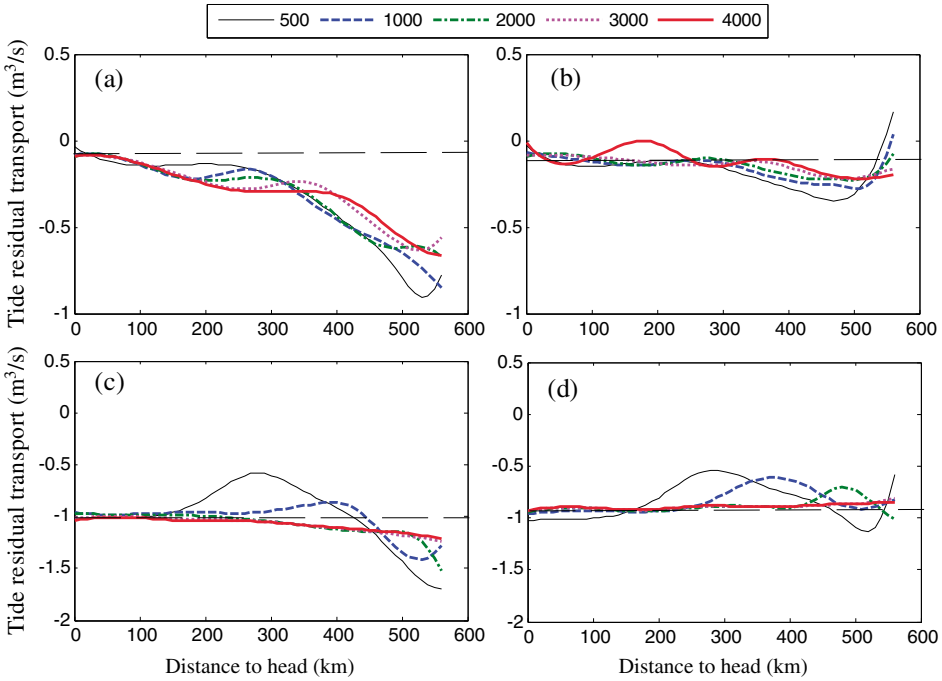

Figure 13. Longitudinal tidal residual sediment transport with morphodynamic evolution for the following cases: (a) river discharge 15,000 m^3/s, no M_4 tide; (b) discharge 30,000 m^3/s, no M_4 tide; (c) river discharge 15,000 m^3/s, with M_4 tide; and (d) discharge 30,000 m^3/s, with M_4 tide in the convergent basin. The thin dashed horizontal lines indicate the equilibrium level.

5.3. Morphodynamic Equilibrium

Morphodynamic equilibrium in tide-dominated estuaries is reached when the residual sediment transport vanishes or in other words when the bed shear stress becomes spatially uniform [*Schramkowski and de Swart*, 2002; *Lanzoni and Seminara*, 2002; *Hibma et al*., 2003b; *van der Wegen et al*., 2008]. In addition, *van der Wegen and Roelvink* [2008] and *van der Wegen et al*. [2008] observed reduced tidal asymmetry strength by morphodynamic development toward equilibrium. Our model results suggest that morphodynamic equilibrium is present in river- and tide-influenced estuaries given a constant discharge. The equilibrium is characterized by a uniform residual sediment transport along the basin (Figure 13) instead of vanishing residual sediment transport. In other words, the gradient in tidal residual sediment transport controls morphodynamic development instead of the sediment transport magnitude itself [*Roelvink and Reniers*, 2011]. The sediment transport magnitude, however, controls the time needed to approach morphodynamic equilibrium.. Morphodynamic equilibrium is reached in a shorter period under higher river discharge conditions because sediment transport rate is larger and spatial gradients in tidal residual sediment transport decreases at a higher rate (Figures 13c and 13d). The persistent residual sediment transport gradient in Figures 13a and 13b indicates that the two scenarios forced by zero and low river discharge may take some more time to reach a morphodynamic equilibrium. Once the equilibrium is reached, the estuary behaves as a sediment transport bypassing conduit conveying the river-supplied sediment seaward, without further net deposition or erosion.

Another way to look at the morphodynamic equilibrium is by a comparison of model results to the empirical relationship between tidal prism (*P*) and cross-sectional area (*A*). Replacing the tidal prism by an ebb tidal volume to take the river discharge into account, we find that the modeled *P-A* relationships at the monitored sections along the estuary are convergent and that they develop toward the empirical line derived on tidal inlets [*Jarrett*, 1976] (Figure 14). Increasing river discharge leads to a larger ebb tidal volume at the same cross-sectional area, suggesting enlarged currents and associated transport capacity. This confirms the universality for a hydraulic geometry relating river discharge or tidal discharge with channel morphology in rivers, tidal basins, and estuaries [*Toffolon and Lanzoni*, 2010; *Sassi et al*., 2012].

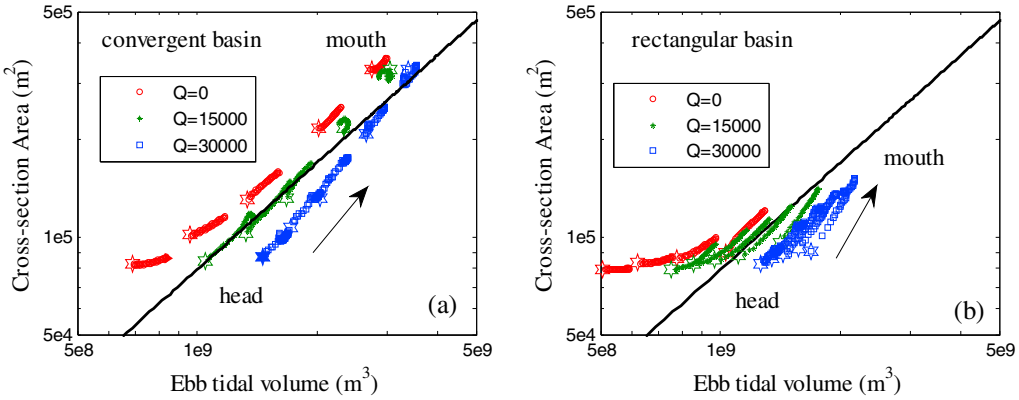

Figure 14. Ebb tidal volume in relationship with cross-section area for the cases without external M_4 tide and river discharge 0, 15,000, and 30,000 m^3/s. The black lines indicate the empirical relationship derived from tidal inlets without jetties by *Jarrett* [1976]. The stars indicate the starting time of each section, and the arrows indicate the variation direction over morphodynamic evolution.

5.4. Implications for Realistic Estuaries

The morphodynamic equilibrium in the schematized simulations is reached under the conditions of constant river discharges and no sea level variations. Results in the 1-D YE model suggest that a dynamic equilibrium may still be present even when the river discharge varies seasonally (see Figure 5). It is unknown how this equilibrium is determined because river flow varies over a large range. High river discharge, reflected by river flood events, can supply a large amount of sediment to an estuary system, damps tides significantly, and thus possibly causes extreme accretion. The impact of seasonal river discharge variations and river flood events on long-term estuarine morphodynamics merit future study.

More tidal constituents are present in reality than the M_2 and M_4 tides we used in this study. One example is the linear interaction between M_2-O_1-K_1 tides which is able to generate tidal residual sediment transport as well [*Hoitink et al*., 2003]. This mechanism differs from M_2-M_4 tidal interaction in that the amplitudes and phases of the astronomical M_2, O_1, and K_1 tides are predetermined, whereas M_4 tide is internally generated and is influenced by river discharge in a manner different from astronomical tides. Moreover, spring-neap tidal variations may have a residual effect on sediment transport [*Allen et al*., 1980]. *Canestrelli et al*. [2013] reported that inclusion of an S_2 tide with an M_2 tide leads to a deeper equilibrium bed profile than the case excluding the S_2 tide, but it is not clear why. In that sense, future study is needed to find out the morphodynamic sensitivity to different tidal constituents and associated tidal interactions.

Mean sea level varies over many time scales (decades to millennia). Sea level rise will reduce the tidal amplitude to water depth ratio and ease landward tidal damping, eventually exerting influences on residual sediment transport and morphodynamic development. *Dissanayake et al*. [2012] and *van der Wegen* [2013] reported that a sea level rise possibly enhances flood tidal asymmetry, decreases intertidal flat area (in 2-D simulations), and drowns tidal basins. Similar sensitivity study considering the balance between riverine sediment supply and sea level variations is needed to explore estuarine morphodynamic adaptation to external forcing changes.

5.5. Shape of Equilibrium Profiles

The equilibrium bed profiles can have large variability depending on the driving forcing and sediment availability in short or long basins [*Friedrichs*, 1995; *de Swart and Zimmerman*, 2009; *Toffolon and Lanzoni*, 2010]. Previous studies reported concave profiles in tide-dominated basins due to divergence of residual sediment transport (Figure 15a) [*Schuttelaars and de Swart*, 2000; *Lanzoni and Seminara*, 2002; *van der Wegen and Roelvink*, 2008]. The concavity varies with the strength of tidal asymmetry and channel geometry. Field observations provide evidences of residual sediment transport divergence by ebb transport dominance at the basin mouth and increasing flood transport dominance in the landward direction in the Tamar Estuary [*Uncles et al*., 1985] and in the Dyfi estuary [*Brown and Davis*, 2010]. Residual sediment transport convergence (inward transport vectors) will lead to a convex equilibrium bed profile. This is the case when an ebb-directed

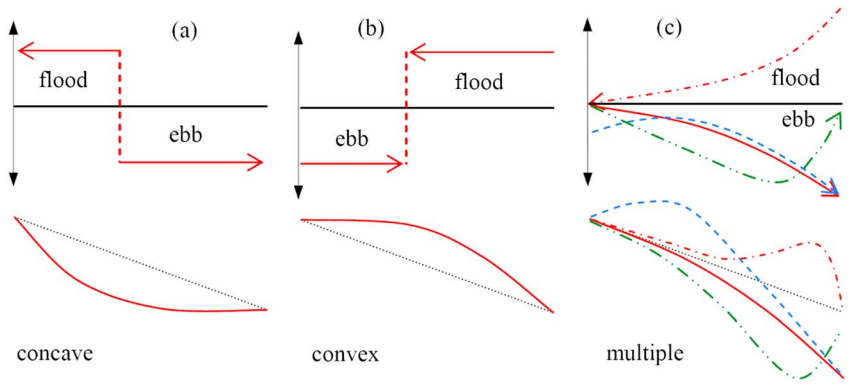

Figure 15. Longitudinal residual sediment transport patterns (top) and corresponding resultant bed profiles (bottom): (a) residual sediment transport divergence with concave profile, (b) residual sediment transport convergence with convex profile, and (c) varying residual sediment transport patterns with complex profiles. The doted lines indicate the initial profile.

residual transport in the upstream part of an estuary driven by a medium river discharge and a flood-directed residual transport downstream induced by a flood tidal asymmetry (Figure 15b). A concave profile can be stable because an associated convergence in minimum shear stress necessary to maintain a zero gradient in residual sediment transport is reached [*Friedrichs*, 1995]. These relationships have some similarities to tidal flat profile dynamics, wherein divergent sediment transport leads to erosion and concavity, while convergent sediment transport leads to accretion and convexity [*Pritchard and Hogg*, 2003].

Equilibrium bed profiles can be complex in shape when the residual sediment transport is unidirectional but with spatially varying gradients (Figure 15c). For instance, a landward decreasing flood tidal asymmetry leads to sediment import and accreted channel bed. A bump or trough in the longitudinal residual sediment transport leads to a corresponding bump or trough in the bed profiles. In summary, it is the residual sediment transport patterns (i.e., the direction and the spatial gradients of the residual sediment transport) that shape the equilibrium bed profiles. Note that the residual sediment transport patterns are a function of basin geometry, hydrodynamic forcing, and sediment properties, as have been discussed by *Friedrichs and Aubrey* [1996] and *Toffolon and Lanzoni* [2010]; hence, the residual sediment transport pattern in realistic estuaries needs specific examination.

6. Conclusions

This study examines 1-D estuarine morphodynamic behavior in river-tide influenced estuaries by applying a morphodynamic model for long-term (in millennia) simulations. The schematized model represents a 560 km long basin with river and tidal forcing comparable to the YE. By sensitivity analysis we explore the morphodynamic impact of basin plan form, tidal asymmetry, and different river discharges. Derived findings are summarized as follows.

1. Morphodynamic equilibrium is reached in river-tide influenced estuaries under constant river discharge. The equilibrium is characterized by uniform tidal residual sediment transport, or in other words vanishing spatial gradients in residual sediment transport, and also by a developing trend toward the empirical relationship between (ebb) tidal volume and cross-sectional area. The time needed to reach morphodynamic equilibrium decreases with increasing river discharges because of enlarged riverine sediment supply and sediment transport rate.
2. Longitudinal residual sediment transport patterns determine the shape of the equilibrium bed profiles under different river and tidal conditions. Convergence and divergence in residual sediment transport lead to convex and concave profiles, respectively. Unidirectional residual sediment transport with seaward increasing or decreasing gradients leads to erosion and accretion and consequent concavity and convexity in bed profiles, respectively.
3. River-tide interaction induces profound tidal residual sediment transport other than the Stokes return flow, tidal asymmetry, and river discharge. River-tide interaction enhances seaward residual sediment transport and stimulates seaward sediment flushing. Interaction between Stokes return flow and tides can

cause a net seaward residual sediment transport despite a flood tidal asymmetry in tide-dominated circumstances.

4. River discharge affects estuarine morphodynamics by supplying sediment, enhancing ebb currents, and interacting with tides. Low river discharge causes deepened bed profiles by enhancing ebb transport. High river discharge induces accreted bed profiles by enlarged sediment supply. This reflects a subtle balance between sediment supply by river flow and sediment flushing (to the sea) by river and tides together. A threshold river discharge can be defined that leads to the deepest equilibrium profile.

Though simple and schematized, this study sheds light on the fundamental role of river discharge and tidal asymmetry on controlling residual sediment transport and long-term estuarine morphodynamic behavior. Future study considering seasonal river discharge variations, more astronomical tidal constituents, and sea level rise is needed.

Acknowledgments

We thank the National Natural Science Foundation of China (41276080), the China Scholarship Council (2009101208), and ReSeDUE project (60038881) for funding this study. Chen Jing (ECNU, Shanghai) and Wan Yuanyang (ECSRC, Shanghai) are thanked for providing parts of bathymetric data in the YE. Ian Townend (University of Southampton/HR Wallingford) and Zhengbing Wang (Delft University of Technology/Deltares) are acknowledged for their constructive comments on this work. The constructive comments from four reviewers and two Editors helped to improve this work greatly.

References

Allen, G. P., J. C. Salomon, P. Bassoullet, Y. D. Penhoat, and C. De Grandpre (1980), Effects of tides on mixing and suspended transport in macrotidal estuaries, *Sediment. Geol.*, *26*(1–3), 69–90.

Brown, J. M., and A. G. Davis (2010), Flood/ebb tidal asymmetry in a shallow sandy estuary and the impact on net sand transport, *Geomorphology*, *114*, 431–439.

Canestrelli, A., S. Lanzoni, and S. Fagherazzi (2013), One-dimensional numerical modeling of the long-term morphodynamic evolution of a tidally-dominated estuary: The lower Fly River (Papua New Guinea), *Sediment. Geol.*, *301*, 107–119.

Chant, R. J., D. Fugate, and E. Garvey (2011), The shaping of an estuarine superfund site: Roles of evolving dynamics and geomorphology, *Estuaries Coasts*, *34*, 90–105.

Chen, J. Y., H. F. Zhu, Y. F. Dong, and J. M. Sun (1985), Development of the Changjiang estuary and its submerged delta, *Cont. Shelf Res.*, *4*(1/2), 47–56.

Cooper, J. A. G. (1993), Sedimentation in a river dominated estuary, *Sedimentology*, *40*, 979–1017.

Cooper, J. A. G. (2002), The role of extreme floods in estuary-coastal behavior: Contrasts between river- and tide-dominated microtidal estuaries, *Sediment. Geol.*, *150*, 123–137.

Dalrymple, R. W., B. A. Zaitlin, and R. Boyd (1992), Estuarine facies models: Conceptual basis and stratigraphic implications—Perspective, *J. Geophys. Res.*, *62*(6), 1130–1146.

de Swart, H. E., and J. T. F. Zimmerman (2009), Morphodynamics of tidal inlet systems, *Annu. Rev. Fluid Mech.*, *41*, 203–229.

Deltares (2011), User manual Delft3D-Flow: Simulation of multi-dimensional hydrodynamic flows and transport phenomena, including sediments. version 3.15, Delft, Netherlands.

Dissanayake, D. M. P. K., R. Ranasinghe, and J. A. Roelvink (2012), The morphological response of large tidal inlet/basin systems to relative sea level rise, *Clim. Change*, *113*, 253–276.

Dronkers, J. (1986), Tide-induced residual transport of fine sediment, in *Proceedings of the Symposium on the Physics of Shallow Bays and Estuaries*, edited by J. van der Kreeke, pp. 228–244, Springer, New York.

Dronkers, J. (2005), *Dynamics of Coastal Systems*, pp. 197–324, World Scientific, Singapore.

Dyer, K. R. (1995), Sediment transport processes in estuaries, in *Geomorphology and Sedimentology of Estuaries*, *Dev. Sedimentol.*, vol. 53, edited by G. M. E. Perillo, pp. 423–449, Elsevier, Amsterdam.

Engelund, F., and E. Hansen (1967), *A Monograph on Sediment Transport in Alluvial Streams*, Teknisk Forlag, Copenhagen.

Fan, D. D., Y. X. Guo, P. Wang, and Z. Shi (2006), Cross-shore variations in the morphodynamic processes of an open-coast mudflat in the Changjiang Delta, China: With an emphasis on storm impacts, *Cont. Shelf Res.*, *26*, 517–538.

Friedrichs, C. T. (1995), Stability shear stress and equilibrium cross-sectional geometry of sheltered tidal channels, *J. Coastal Res.*, *11*(4), 1062–1074.

Friedrichs, C. T., and D. G. Aubrey (1988), Non-linear tidal distortion in shallow well-mixed estuaries: A synthesis, *Estuarine Coastal Shelf Sci.*, *27*, 521–545.

Friedrichs, C. T., and D. G. Aubrey (1994), Tidal propagation in strongly convergent channels, *J. Geophys. Res.*, *99*, 3321–3336.

Friedrichs, C. T., and D. G. Aubrey (1996), Uniform bottom shear stress and equilibrium hypsometry of intertidal flats, in *Mixing in Estuaries and Coastal Seas*, *Coastal and Estuarine Studies*, vol. 50, edited by C. Pattiaratchi, pp. 405–429, AGU, Washington D. C.

Gallo, M. N., and S. B. Vinzon (2005), Generation of overtides and compound tides in the Amazon estuary, *Ocean Dyn.*, *55*, 441–448.

Gao, S., and M. Collins (1994), Tidal inlet equilibrium, in relation to cross-sectional area and sediment transport patterns, *Estuarine Coastal Shelf Sci.*, *38*(2), 157–172.

Garel, E., L. Pinto, A. Santos, and O. Ferreira (2009), Tidal and river discharge forcing upon water and sediment circulation at a rock-bound estuary, *Estuarine Coastal Shelf Sci.*, *84*, 269–281.

Godin, G. (1985), Modification of river tides by the discharge, *J. Waterw. Port Coastal Ocean Eng.*, *111*(2), 257–274.

Hibma, A., H. J. de Vriend, and M. J. F. Stive (2003a), Numerical modeling of shoal pattern formation in well-mixed elongated estuaries, *Estuarine Coastal Shelf Sci.*, *57*, 981–991.

Hibma, A., H. M. Schuttelaars, and Z. B. Wang (2003b), Comparison of longitudinal equilibrium profiles of estuaries in idealized and process-based models, *Ocean Dyn.*, *53*, 252–269.

Hibma, A., M. J. F. Stive, and Z. B. Wang (2004), Estuarine morphodynamics, *Coastal Eng.*, *8–9*, 765–778.

Hoitink, A. J. F., P. Hoekstra, and D. S. van Maren (2003), Flow asymmetry associated with astronomical tides: Implications for the residual transport of sediment, *J. Geophys. Res.*, *108*(C10), 3315, doi:10.1029/2002JC001539.

Horrevoets, A. C., H. H. G. Savenije, J. N. Schuurman, and S. Graas (2004), The influence of river discharge on tidal damping in alluvial estuaries, *J. Hydrol.*, *294*(4), 213–228.

Jarrett, J. T. (1976), Tidal prism—Inlet area relationships, *GITI Rep. 3*, Coastal Eng. Res. Cent., US Army Corps of Engineers, Fort Belvoir, Va.

Jay, D. A. (1991), Green's law revisited: Tidal long-wave propagation in channels with strong topography, *J. Geophys. Res.*, *96*, 20,585–20,598.

Karunarathna, H. (2010), Modeling the long-term morphological evolution of the Clyde Estuary, Scotland, U. K., *J. Coast Conserv.*, doi:10.1007/s11852-010-0138-8.

Lanzoni, S., and G. Seminara (1998), On tide propagation in convergent estuaries, *J. Geophys. Res.*, *103*(C13), 30,793–30,812.
Lanzoni, S., and G. Seminara (2002), Long-term evolution and morphodynamic equilibrium to tidal channels, *J. Geophys. Res.*, *107*(C1), 3001, doi:10.1029/2000JC000468.
LeBlond, P. H. (1991), Tides and their interactions with other oceanographic phenomena in shallow water (review), in *Tidal Hydrodynamics*, edited by B. B. Parker, pp. 357–378, John Wiley, New York.
Leopold, L. B., M. G. Wolman, and J. P. Miller (1964), *Fluvial Processes in Geomorphology*, pp. 215–227, W. H. Freeman, San Francisco, Calif.
Lesser, G. R., J. A. Roelvink, J. A. T. M. van Kester, and G. S. Stelling (2004), Development and validation of a three-dimensional morphological model, *Coastal Eng.*, *51*, 883–915.
Li, C. Y., and J. O'Donnell (2005), The effect of channel length on the residual circulation in tidally dominated channels, *J. Phys. Oceanogr.*, *35*, 1826–1840.
Li, J. (2004), Tidal limit and tidal current limit & response to major engineering in Yangtze Estuary, MS thesis of East China Normal Univ., Shanghai, China.
Liu, H., Q. He, Z. B. Wang, G. J. Weltje, and J. Zhang (2010), Dynamics and spatial variability of near-bottom sediment exchange in the Yangtze Estuary, China, *Estuarine Coastal Shelf Sci.*, *86*, 322–330.
Liu, J. P., A. C. Li, K. H. Xu, D. M. Velozzi, Z. S. Yang, J. D. Milliman, and D. J. DeMaster (2006), Sedimentary features of the Yangtze River-derived along-shelf clinoform deposit in the East China Sea, *Cont. Shelf Res.*, *26*, 2141–2156.
Moore, R. D., J. Wolf, A. J. Souza, and S. S. Flint (2009), Morphological evolution of the Dee estuary, eastern Irish Sea, UK: A tidal asymmetry approach, *Geomorphology*, *103*, 588–596.
Nittrouer, J. A., J. Shaw, M. P. Lamb, and D. Mohrig (2011), Spatial and temporal trends for water-flow velocity and bed material sediment transport in the lower Mississippi River, *Geol. Soc. Am. Bull.*, *124*, 400–414.
O'Brien, M. P. (1969), Equilibrium flow areas of tidal inlets on sandy coasts, *J. Waterw. Harbors*, *95*, 43–52.
Parker, B. B. (1991), The relative importance of the various nonlinear mechanisms in a wide range of tidal interactions, in *Tidal Hydrodynamics*, edited by B. B. Parker, pp. 237–268, John Wiley, New York.
Postma, H. (1961), Transport and accumulation of suspended matter in the Dutch Wadden Sea, *Neth. J. Sea Res.*, *1*, 148–190.
Powell, M. A., R. J. Thieke, and A. J. Mehta (2006), Morphodynamic relationships for ebb and flood delta volumes at Florida's tidal entrances, *Ocean Dyn.*, *56*, 295–307.
Prandle, D. (1985), Classification of tidal response in estuaries from channel geometry, *Geophys. J. R. Astron. Soc.*, *80*, 209–221.
Pritchard, D., and A. J. Hogg (2003), Cross-shore sediment transport and the equilibrium morphology of mudflats under tidal currents, *J. Geophys. Res.*, *108*(C10), 3313, doi:10.1029/2002JC001570.
Roelvink, J. A. (2006), Coastal morphodynamic evolution techniques, *Coastal Eng.*, *53*, 177–187.
Roelvink, J. A., and A. Reniers (2011), *A Guide to Modeling Coastal Morphology*, pp. 145–167, Word Scientific, Singapore.
Sassi, M. G., and A. J. F. Hoitink (2013), River flow controls on tides and tide-mean water level profiles in a tidal freshwater river, *J. Geophys. Res. Ocean*, *118*, 1–13, doi:10.1002/jgrc.20297.
Sassi, M. G., A. J. F. Hoitink, B. de Brye, and E. Deleersnijder (2012), Downstream hydraulic geometry of a tidally influenced river delta, *J. Geophys. Res.*, *117*, F04022, doi:10.1029/2012JF002447.
Savenije, H. H. G. (2005), *Salinity and Tides in Alluvial Estuaries*, Elsevier Science, Amsterdam, Netherlands.
Schramkowski, G. P., and H. E. de Swart (2002), Morphodynamic equilibrium in straight tidal channels: Combined effects of the Coriolis force and external overtides, *J. Geophys. Res.*, *107*(C12), 3227, doi:10.1029/2000JC000693.
Schramkowski, G. P., H. M. Schuttelaars, and H. E. de Swart (2002), The effect of geometry and bottom friction on local bed forms in a tidal embayment, *Cont. Shelf Res.*, *22*, 1821–1833.
Schramkowski, G. P., H. M. Schuttelaars, and H. E. de Swart (2004), Non-linear channel-shoal dynamics in long tidal embayments, *Ocean Dyn.*, *54*, 399–407.
Schuttelaars, H. M., and H. E. de Swart (1996), An idealized long-term morphodynamic model of a tidal embayment, *Eur. J. Mech. B. Fluids*, *15*, 55–80.
Schuttelaars, H. M., and H. E. de Swart (2000), Multiple morphodynamic equilibria in tidal embayments, *J. Geophys. Res.*, *105*, 24,105–24,118.
Speer, P. E., and D. G. Aubrey (1985), A study of non-linear tidal propagation in shallow inlet/estuarine systems. Part II: Theory, *Estuarine Coastal Shelf Sci.*, *21*, 207–224.
Stokes, G. G. (1847), On the theory of oscillatory waves, *Trans. Cambridge Philos. Soc.*, *8*, 441–455.
Todeschini, I., M. Toffolon, and M. Tubino (2008), Long-term morphological evolution of funnel-shape tide-dominated estuaries, *J. Geophys. Res.*, *113*, C05005, doi:10.1029/2007JC004094.
Toffolon, M., and S. Lanzoni (2010), Morphological equilibrium of short channels dissecting the tidal flats of coastal lagoons, *J. Geophys. Res.*, *115*, F04036, doi:10.1029/2010JF001673.
Townend, I. (2005), An examination of empirical stability relationship for UK estuaries, *J. Coastal Res.*, *21*(5), 1042–1053.
Uncles, R. J., R. C. A. Elliott, and S. A. Weston (1985), Lateral distributions of water, salt and sediment transport in a partly mixed estuary, in *Proceedings of the 19th International Conference on Coastal Engineering*, edited by B. L. Edge, pp. 3067–3077, Am. Soc. of Civil Engineers, New York.
van de Kreeke, J. (1998), Adaptation of the Frisian Inlet to a reduction in basin area with special references to the cross-sectional area of the inlet channel, in *Physics of Estuarine and Coastal Seas*, edited by J. Dronkers and M. B. A. M. Scheffers, pp. 355–362, Balkema, Rotterdam, Netherlands.
van de Kreeke, J., and K. Robaczewska (1993), Tide-induced residual transport of coarse sediment: Application to the Ems Estuary, *Neth. J. Sea Res.*, *31*(3), 209–220.
van der Wegen, M. (2013), Numerical modeling of the impact of sea level rise on tidal basin morphodynamics, *J. Geophys. Res. Earth Surf.*, *118*, 447–460, doi:10.1002/jgrf.20034.
van der Wegen, M., and J. A. Roelvink (2008), Long-term morphodynamic evolution of a tidal embayment using a two-dimensional, process-based model, *J. Geophys. Res.*, *113*, C03016, doi:10.1029/2006JC003983.
van der Wegen, M., and J. A. Roelvink (2012), Reproduction of estuarine bathymetry by means of a process-based model: Western Scheldt case study, the Netherlands, *Geomorphology*, *179*, 52–167.
van der Wegen, M., Z. B. Wang, H. H. G. Savenije, and J. A. Roelvink (2008), Long-term morphodynamic evolution and energy dissipation in a coastal plain, tidal embayment, *J. Geophys. Res.*, *113*, F03001, doi:10.1029/2007JF000898.
van der Wegen, M., A. Dastgheib, and J. A. Roelvink (2010), Morphodynamic modelling of tidal channel evolution in comparison to empirical PA relationship, *Coastal Eng.*, *57*, 827–837.
van Dongeren, A. R., and H. J. de Vriend (1994), A model of morphological behaviour of tidal basins, *Coastal Eng.*, *22*, 287–310.

van Rijn, L. C. (2011), *Principles of Fluid Flow and Surface Waves in Rivers, Estuaries, Seas and Oceans*, pp. 8.73–8.92, Aqua publications, Amsterdam, Netherlands.

Wang, Z. B., H. Juken, and H. J. de Vriend (1999), Tidal asymmetry and residual sediment transport in estuaries, *WL|Hydraul., Rep. Z2749*, Delft, Netherlands.

Xue, P. F., C. S. Chen, P. X. Ding, R. C. Beardsley, H. C. Lin, J. Z. Ge, and Y. Z. Kong (2009), Saltwater intrusion into the Changjiang River: A model-guided mechanism study, *J. Geophys. Res.*, *114*, C02006, doi:10.1029/2008JC004831.

Yun, C. X. (2004), *Recent Evolution of the Yangtze Estuary and Its Mechanism* [in Chinese], China Ocean Press, Beijing.

Zhang, E. F., X. Q. Chen, and X. L. Wang (2010), Water discharge changes of the Changjiang River downstream Datong during dry season, *J. Geogr. Sci.*, *13*(3), 355–362.